

Ground state configurations of vortices in superconducting film with magnetic dot

Zoran Ristivojevic

Institut für Theoretische Physik, Universität zu Köln, Zùlpicher Straße 77, D-50937 Köln, Germany

(Dated: 12-02-2022 12:22)

We consider a thin superconducting film with a magnetic dot with permanent magnetization (normal to the film) placed on it by a method based on London-Maxwell equations. For sufficiently high dot magnetization a single vortex appears in the ground state. Further increase of magnetization is accompanied with the appearance of antivortices and more vortices in the film. We study analytically conditions for the appearance of a vortex–antivortex pair for a range of parameters. The phase diagram with diversity of vortex–antivortex states is calculated numerically. When appear in the ground state, antivortices are at distances comparable to the dot radius. For not too large dot radii the total vorticity in the ground state is predominantly zero or one. Magnetic field due to the dot and vortices everywhere in space is calculated analytically.

PACS numbers: 74.81.-g,75.70.-i,74.25.Dw,74.78.-w

I. INTRODUCTION

Type-II superconductors in an external homogeneous magnetic field are much studied and well understood.^{1,2} They accommodate regularly distributed flux tubes–vortices for fields between the lower and the upper critical field.³ Similar situation occurs in type-II superconducting films in perpendicular fields.^{4,5} A difference is that the first critical field for films vanishes for macroscopically large samples.^{5,6}

An interesting class of systems which have attracted a great attention only recently are ferromagnet–superconductor hybrid systems. There one examines the influence of a material with heterogeneous magnetization on a superconductor.⁷ Direct contact between the magnetic material and the superconductor is avoided usually by a thin insulating layer which suppresses the proximity effect. These hybrid systems can be fabricated fully controlling their parameters.⁸ Inhomogeneous magnetization of ferromagnets generates magnetic field that penetrates the superconductor. As a response to that field, supercurrents (and vortices under certain conditions) are induced in the film. The magnetic field of supercurrents interacts with the magnetic subsystem. Therefore by tuning parameters of the magnetic subsystem we examine different phenomena of the composite system. Hybrid systems offer a number of realizations of new interesting phenomena which include pinning of magnetization induced vortices, commensurability effects (between external magnetic field and periodic structure of magnetic material) on the superconductor resistivity and others.^{7,8,9,10}

In this paper we are focused on the simplest ferromagnet–superconductor hybrid system which consists of a single magnetic dot grown on top of a type-II superconducting film. The magnetic dot is assumed to have permanent magnetization normal to the film surface. Despite its simplicity this system deserves attention since a diversity of different ground states can be realized in the parameter space. Dots with sufficiently small magnetization produce only supercurrents in the

film, while with the increase of magnetization different configurations of vortex states appear in the ground state(GS).^{11,12,13,14,15,16} This is in striking contrast with respect to films in homogeneous fields.^{5,6} However, we expect that for large dot radii any magnetization induces vortices in the film, like the case with homogeneous magnetic field.

The main goal in this paper is to define regions in the parameter space with different ground state configurations of vortices. A possible question that is under debate in literature is whether antivortices may also be induced in the film. One finds different statements about the presence of antivortices: while some authors claim its existence,^{12,15,17} the others do not find it.^{13,14} We think that rough estimates in Ref.¹², calculations with magnetic dipole in Ref.¹⁷ or study inside the nonlinear Ginzburg–Landau theory with restriction to zero total vorticity states done in Ref.¹⁵ are insufficient, and offer an independent and detailed study of this problem. Under which conditions and where vortices and antivortices appear will be answered in our paper.

Magnetization of the dot (which is normal to the film surface) produces magnetic field in the film, which is under the dot parallel to the magnetization, but antiparallel for larger distances than the dot radius. The magnetic field under the dot favors the appearance of vortices under the dot, the appearance of antivortices outside the dot. Whether some vortex–antivortex configuration have the smallest energy or not depends on details of the interaction energy.

Vortices have spatial structure and the superconducting order parameter vanishes roughly at distances smaller than ξ around the center of the vortex. Here ξ denotes the coherence length of a superconductor.¹ The nonlinear Ginzburg–Landau approach takes this into account, but apart from numerical treatment one can hardly get analytic results.¹⁵ Our approach is based on London–Maxwell equations.^{13,18} Despite its simplicity (it treats vortices as point objects) it an useful approach since one may get analytic expressions for relevant quantities which are asymptotically exact when all lengths in the problem

are larger than the spatial vortex extension.

It is interesting to mention that the vortex nucleation in superconducting microtriangles and squares occurs in such a way that the symmetry of the superconductor is preserved.^{19,20} For example in the case of a triangle, the state with total vorticity two is realized with three vortices and a single antivortex in the center of the triangle and preserves C_3 symmetry. Our system with infinite superconducting film and with magnetic dot on top of it has rotational C_∞ symmetry around the dot center. This symmetry is reduced in the presence of vortices and antivortices contrary to the abovementioned example. For the most possible symmetric states with total vorticity zero the rotational symmetry is either reduced to discrete C_N symmetry (for the case of $N \geq 2$ single vortices and antivortices) or does not exist at all (for a vortex–antivortex pair). When two and more (we have checked up to four) vortices and antivortices are present in the zero vorticity state, vortices are distributed in a symmetric fashion around the dot center while antivortices are outside the dot in the same manner, like homothetically transformed vortices. In the case of a single vortex–antivortex pair, the dot’s center, vortex and antivortex are collinear. Other states with nonzero vorticity are less symmetric. When the number of antivortices is five and more, they may form shells around a central vortex in zero vorticity states.¹⁵

The rest of the paper is organized as follows: in section II we introduce a theoretical model we use to describe the system. We calculate analytically the interaction energy between a cylindrical magnetic dot and vortices in the film. In section III we determine analytically conditions for the ground state configurations that consist of a single vortex and a vortex–antivortex pair, as well as separatrices between those ground states. Positions of vortices are also found. Magnetic field in whole space and supercurrents in the film are calculated in section IV. Numerical results for the phase diagram with diversity of vortex–antivortex configurations as well as their positions are presented in Section V. Section VI contains numerical estimates of the parameters and conclusions.

Some technical details are relegated for the appendix.

II. MODEL

We consider a circular magnetic dot of radius R and thickness a_t placed above the infinite superconducting film at distance d with its basis parallel to the film surface. The dot magnetization M is assumed to be constant and normal to the film surface, see Fig. 1. Apart from the supercurrents, the dot may also induce vortices and antivortices in the film. We will study these vortex configurations. Since our problem has many parameters there are many regions in the parameter space which may have different ground state configurations(GSC). The GSC here denotes a configuration of vortices in the film with lowest energy. Among all possible GSCs a trivial one has no vortices. This is expected for sufficiently small magnetization. With increasing M the appearance of vortices is energetically favorable.

We assume quite generally that our system consists of N vortices with vorticities n_i at positions $\boldsymbol{\rho}_i$ for a given magnetization M . The energy of the system is

$$E_{n_1, \dots, n_N} = \sum_{i=1}^N n_i^2 U_v + \sum_{i < j}^N n_i n_j U_{vv}(\rho_{ij}) + \sum_{i=1}^N n_i U_{mv}(\rho_i), \quad (1)$$

where $\rho_{ij} = |\boldsymbol{\rho}_i - \boldsymbol{\rho}_j|$ and $\rho_i = |\boldsymbol{\rho}_i|$. U_v is the single vortex energy, U_{vv} is the vortex–vortex interaction, and U_{mv} is the vortex–magnet interaction. For a given magnetization of the dot, the system will be in the state where E_{n_1, \dots, n_N} is minimal. Expression (1) assumes that the system in the trivial ground state has zero energy $E_0 = 0$.

U_{mv} and U_{vv} can be calculated by using the approach developed in^{13,18} based on London–Maxwell equations. Here we only quote final results. For the interaction energy between the dot and a vortex with vorticity n placed at distance ρ from the dot’s center we get

$$U_{mv}(\rho, n) = -nMR\phi_0 \int_0^\infty dx J_0\left(\frac{\rho}{R}x\right) J_1(x) \frac{1}{1 + 2\frac{\lambda}{R}x} \frac{\exp\left(-\frac{d}{R}x\right) - \exp\left(-\frac{d+a_t}{R}x\right)}{x}, \quad (2)$$

where J_0 and J_1 are the Bessel functions of the first kind. λ is the effective penetration depth and is equal λ_L^2/d_s , where λ_L is the London penetration depth and d_s the film thickness. The film thickness is assumed to satisfy $d_s \ll \lambda_L$ and accordingly the magnetic field and currents are uniform through the thickness of the film. Expression (2) has the following behavior in some regions (we take $d = 0$ for simplicity):

$$U_{mv}(\rho, n) = -nMa_t\phi_0 \frac{R}{4\lambda} \begin{cases} 2 - \frac{\rho^2}{2R^2}, & \rho \ll a_t \ll R \ll \lambda \\ \frac{R}{2a_t} + \frac{R}{a_t} \ln \frac{2a_t}{R} - \frac{\rho^2}{2Ra_t}, & \rho \ll R \ll a_t \ll \lambda \\ \frac{R}{2\lambda} \left(\frac{2\lambda}{\rho} + \ln \frac{\rho}{4\lambda} + \gamma \right), & a_t, R \ll \rho \ll \lambda \\ \frac{4\lambda^2 R}{\rho^3}, & a_t, R \ll \lambda \ll \rho \end{cases} \quad (3)$$

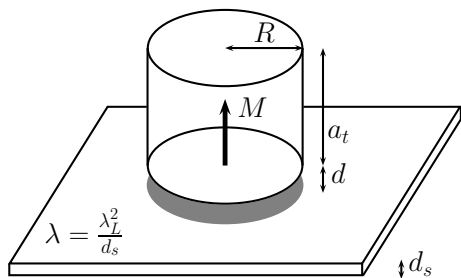


FIG. 1: Magnetic dot with perpendicular permanent magnetization M upon infinite superconducting film.

Some technical details for obtaining (3) are presented in the appendix.

The interaction between vortices of vorticities n_1 and n_2 separated by a distance ρ is given by

$$U_{vv}(\rho) = \frac{n_1 n_2 \phi_0^2}{16\pi\lambda} \left[H_0\left(\frac{\rho}{2\lambda}\right) - Y_0\left(\frac{\rho}{2\lambda}\right) \right], \quad (4)$$

which has asymptotic forms

$$U_{vv}(\rho) = n_1 n_2 \begin{cases} 2U_v, & \rho \ll \xi \ll \lambda \\ \frac{\phi_0^2}{8\pi^2\lambda} \left(\ln \frac{4\lambda}{\rho} - \gamma \right), & \xi \ll \rho \ll \lambda \\ \frac{\phi_0^2}{4\pi^2} \frac{1}{\rho}, & \lambda \ll \rho \end{cases} \quad (5)$$

In previous expressions ϕ_0 is the magnetic flux quantum. H_0 is the Struve function of order zero and Y_0 is the Bessel function of the second kind of order zero.²¹ U_v is the single vortex energy²²

$$U_v = \frac{\phi_0^2}{16\pi^2\lambda} \left(\ln \frac{4\lambda}{\xi} - \gamma \right), \quad (6)$$

where $\gamma \approx 0.577$ is the Euler constant. Two vortices which centers are at distances smaller than ξ are considered in our model as a double vortex. Its total energy is $4U_v$: from two single vortices comes $2U_v$ as well as from their interaction. In the same way a vortex–antivortex pair at distances smaller than ξ does not exist, i.e. it is annihilated. Here we mention that Eqs. (4) and (6) are valid for films with lateral dimensions much larger than the effective penetration depth. In the opposite case the lateral system size enters expressions (4) and (6) instead of λ . This change does not complicate further considerations and we do not consider such situation.

In the following we will use energy expression (1) which will be minimized in the parameter space and which determines the structure of vortex configurations in the GS.

III. GROUND STATES WITH VORTICES

To get further insight into possible GSCs of the system with respect to different parameters, we consider asymptotic forms of Eqs. (2) and (4). To simplify expressions we will just consider the case of thin magnetic dots ($a_t < R$)

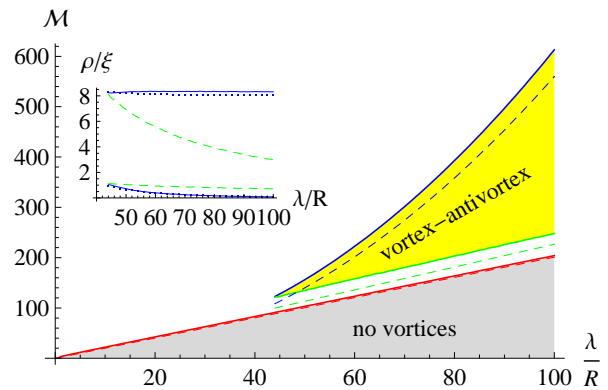


FIG. 2: (Color online) Phase diagram of a magnetic dot for $L = 6$ and $a_t/R = 0.01$: vortex–antivortex state appears for large enough dot magnetization and large enough λ/R . Solid lines are obtained numerically, while dashed are analytic formulae (7), (9) and (10) with $A = 1.7$. Inset: upper(lower) curves show antivortex(vortex) positions. Solid (Dashed) lines correspond to the upper (lower) phase boundary of the vortex–antivortex pair. Dotted lines are plotted using analytic formulae (12) and (13).

placed at the film surface ($d = 0$). The other cases may be straightforwardly done having the asymptotic forms of U_{mv} .

Necessary condition for the appearance of an extra vortex with respect to the trivial GSC is $E_1 \leq E_0$. Using (3) in the lowest order in λ/R we get

$$\mathcal{M} \geq \frac{2\lambda}{R}. \quad (7)$$

Here we have introduced $\mathcal{M} = Ma_t\phi_0/U_v$. This result agrees with one from Ref.¹³. Here we have taken into account that the strongest attraction energy between single vortex and magnet occurs at $\rho = 0$. The phase boundary is a linear function of λ/R for $R < \lambda$. For large dot radii R , result (7) shows that any nonzero magnetization induces a vortex in the film. This resembles the result for vanishing of the first critical field for thin films in an external homogeneous magnetic field.^{5,6}

Apart from the trivial GSC and the single vortex state, there are other states for higher \mathcal{M} . We will now determine a portion of the parameter space where a vortex–antivortex pair appears in the GS. We found that such possibility is only briefly mentioned in literature,^{12,17} or disproved.¹⁴ We will try to clarify this issue giving explicit expressions for the phase boundary and for the vortex and antivortex positions.

The energy $E_{1,-1}$ of a vortex–antivortex pair separated by ρ ($\rho \ll 2\lambda$) with vortex under the dot center reads

$$\begin{aligned} \frac{E_{1,-1}(\rho)}{U_v} = & 2 + \frac{U_{mv}(0,1)}{U_v} + \mathcal{M} \frac{R^2}{4\lambda\rho} \\ & - \left(\frac{2}{L} + \mathcal{M} \frac{R^2}{8\lambda^2} \right) \left(\ln \frac{4\lambda}{\rho} - \gamma \right), \end{aligned} \quad (8)$$

where L is the logarithmic factor in the vortex self energy $L = \ln(4\lambda/\xi) - \gamma$. We may notice from Eq. (8) that the main contribution from the magnetic dots on the antivortex is the energy cost which scales with the distance from the dot as $1/\rho$, while the energy gain due to the vortex–antivortex attraction scales logarithmically which may lead to a stable potential minimum for some parameters. For that energy minimum we get that it occurs at $\rho^* = 2\lambda/(1 + \frac{2}{L} \frac{8\lambda^2}{\mathcal{M}R^2})$ which should be supplemented with the self consistency condition $\rho^* \ll \lambda$ where Eq. (8) is valid and also $\rho^* > a_t, R$. Implicit equation $E_{1,-1}(\rho^*) = 0$ defines the phase boundary for the creation of a vortex–antivortex pair. In addition if $E_{1,-1}(\rho^*) < E_1$ and $E_{1,-1} < 0$ are satisfied the vortex–antivortex pair forms the GS. Condition $E_{1,-1} \leq E_1$ gives

$$\mathcal{M} \leq \frac{\lambda^2}{R^2} \frac{32}{L \left[\exp \left(1 + \gamma + \frac{L}{2} \right) - 2 \right]}, \quad (9)$$

which is the upper dashed line for vortex–antivortex phase boundary in Fig. 2. Another phase boundary we get from the condition that the antivortex is outside the dot $\rho^* \geq AR$ which gives

$$\mathcal{M} \geq \frac{8}{L} \frac{\lambda}{R} A \quad (10)$$

with some number A of order one.

From the last two inequalities we get a condition on λ/R when the vortex–antivortex forms the GS (in the case $a_t < R, d = 0$):

$$\frac{\lambda}{R} \geq \frac{A}{4} \left[\exp \left(1 + \gamma + \frac{L}{2} \right) - 2 \right]. \quad (11)$$

In Eq. (8) we have assumed that the vortex position is under the dot $\rho_1 = 0$ for simplicity. Having in mind relatively flat magnet–vortex interaction (3) for $\rho < R$ the system can gain even more energy allowing $\rho_1 > 0$ toward antivortex, since the energy loss in the vortex–magnet interaction may be overcompensated by the vortex–antivortex interaction. A similar calculation to the previous one gives for the vortex displacement

$$\frac{\rho_1}{R} = \frac{64\lambda^2}{\mathcal{M}^2 R^2 L^2} \quad (12)$$

while for the antivortex

$$\frac{\rho}{2\lambda} = \frac{1}{1 + \frac{2}{L} \frac{8\lambda^2}{\mathcal{M}R^2}} - \frac{2R}{\mathcal{M}L\lambda}, \quad (13)$$

and the center of the dot, vortex and antivortex are collinear. Physically we see that stronger the magnetization of the dot, the vortex is closer to dot's center, which

is expected. What we also see is that the symmetry of a single vortex GSC is violated for the range of parameters where the antivortex appears.

IV. MAGNETIC FIELD

Magnetic dot on top of a superconducting film induces circular supercurrents in the film. These currents generate magnetic field in and outside the film. Total magnetic field in space is a sum of three terms: due to supercurrents, due to the dot and due to vortices. In this section we calculate the magnetic field using the approach developed in^{13,18}. The presence of vortices in the film may be observed by measuring the magnetic field and its behavior near the film surface, since vortices change the magnetic field dependence of radial separation from the dot's center.

A vortex of vorticity n produces normal to the film surface (axial) and parallel the film surface (radial) magnetic field which respectively read²³

$$B_z^v(\rho, z) = \frac{n\phi_0}{2\pi} \int_0^\infty dk \frac{k \exp(-k|z|)}{1 + 2\lambda k} J_0(k\rho), \quad (14)$$

$$B_{\parallel}^v(\rho, z) = \frac{n\phi_0}{2\pi} \frac{|z|}{z} \int_0^\infty dk \frac{k \exp(-k|z|)}{1 + 2\lambda k} J_1(k\rho). \quad (15)$$

The previous expressions at the film surface $z = 0$ have the following asymptotic forms:

$$B_z^v(\rho, 0) = \frac{n\phi_0}{8\pi\lambda^2} \begin{cases} \frac{2\lambda}{\rho}, & \rho \ll \lambda \\ \left(\frac{2\lambda}{\rho} \right)^3, & \lambda \ll \rho \end{cases} \quad (16)$$

$$B_{\parallel}^v(\rho, z \rightarrow 0) = \frac{n\phi_0}{8\pi\lambda^2} \frac{|z|}{z} \begin{cases} \frac{2\lambda}{\rho}, & \rho \ll \lambda \\ \left(\frac{2\lambda}{\rho} \right)^2, & \lambda \ll \rho \end{cases} \quad (17)$$

The parallel magnetic field outside the film (remember that in our calculations the film is just in $z = 0$ plane) changes the sign going from one side of the film to another. This is due to the fact that the vortex induces currents in the film which circulate around it, and jump in B_{\parallel}^v crossing the film surface is the condition for the jump at the boundaries in electrodynamics due to surface currents.²⁴ Normal magnetic field is continuous across the film. The surface current density K_v produced by the vortex is given by

$$\mathbf{K}_v = \frac{c}{4\pi} \mathbf{e}_z \times (\mathbf{B}_{\parallel}^v(\rho, 0^+) - \mathbf{B}_{\parallel}^v(\rho, 0^-)), \quad (18)$$

where c is the velocity of light.

The magnetic field due to the dot is given by two integrals:

$$B_z^d(\rho, z) = -2\pi MR \int_0^\infty dk J_0(k\rho) J_1(kR) \left\{ \frac{\exp(-k(|z| + d))}{1 + 2\lambda k} [1 - \exp(-ka)] \right. \\ \left. + \text{sign}(d - z) [1 - \exp(-k|d - z|)] - \text{sign}(d + a - z) [1 - \exp(-k|d + a - z|)] \right\}, \quad (19)$$

$$B_{\parallel}^d(\rho, z) = -2\pi MR \int_0^\infty dk J_1(k\rho) J_1(kR) \left\{ \text{sign}(z) \frac{\exp(-k(|z| + d))}{1 + 2\lambda k} [1 - \exp(-ka)] \right. \\ \left. + \exp(-k|d - z|) - \exp(-k|d + a - z|) \right\}. \quad (20)$$

Eq. (19)(Eq. (20)) we write as a sum $B_{z(\parallel)}^d = B_{z(\parallel)}^{dm} + B_{z(\parallel)}^{df}$ of fields due to the dot $B_{z(\parallel)}^{dm}$ and due to the supercurrents $B_{z(\parallel)}^{df}$. $B_{z(\parallel)}^{dm}$ is formally defined by setting $\lambda \rightarrow \infty$ in Eq. (19)(Eq. (20)) which means the system with the dot and without the film. We evaluate (19) and (20) for $d = 0$ and at the film surface. Purely magnetic terms are given by

$$B_z^{dm}(\rho, 0) = -\pi MR^2 a_t \frac{1}{\rho^3}, \quad (21)$$

$$B_{\parallel}^{dm}(\rho, 0) = -\pi MR^2 a_t \frac{3a_t}{2\rho^4}, \quad (22)$$

to the leading order for $\rho \gg a_t, R$. The previous result can be understood as the magnetic dipolar field.²⁴ The part due to supercurrents is

$$B_z^{df}(\rho, 0) = -\pi MR^2 a_t \begin{cases} \frac{1}{4\lambda\rho^2}, & a_t, R \ll \rho \ll \lambda \\ \mathcal{O}\left(\frac{1}{\rho^4}\right), & a_t, R \ll \lambda \ll \rho \end{cases} \quad (23)$$

$$B_{\parallel}^{df}(\rho, z \rightarrow 0) = -\pi MR^2 a_t \frac{|z|}{z} \begin{cases} \frac{1}{\lambda\rho^2}, & a_t, R \ll \rho \ll \lambda \\ \frac{6\lambda}{\rho^4}, & a_t, R \ll \lambda \ll \rho \end{cases} \quad (24)$$

Again parallel field B_{\parallel}^{df} jumps across the film surface due to surface currents. The surface current density K_m in the film due to the presence of the dot is given by

$$\mathbf{K}_m = \frac{c}{4\pi} \mathbf{e}_z \times (\mathbf{B}_{\parallel}^{df}(\rho, 0^+) - \mathbf{B}_{\parallel}^{df}(\rho, 0^-)). \quad (25)$$

As first proposed in Ref.¹³ the presence of a single vortex in the film can be proved by observing the change of sign of the total field B_z near the film. We can now calculate that it happens when $B_z^d(\rho_{sz}, 0) + B_z^v(\rho_{sz}, 0) = 0$ or at $\rho_{sz} = 2\pi\sqrt{MR^2 a_t \lambda / \phi_0}$ provided a single vortex appears in the GS. Using the condition for the single vortex (7) we get $\rho_{sz} \approx \sqrt{LR\lambda/2}$. We can also formulate a similar condition for the presence of a single vortex but for the parallel field, which also changes sign for at distance $\rho_{s\parallel}$ from the dot defined by $B_{\parallel}^d(\rho_{s\parallel}, 0) + B_{\parallel}^v(\rho_{s\parallel}, 0) = 0$. The solution of the resulting cubic equation is $\rho_{s\parallel} \approx (6\pi^2 MR^2 a_t^2 \lambda / \phi_0)^{1/3}$ above the film ($z \rightarrow 0^+$), which using (7) becomes $\rho_{s\parallel} \approx (3LRa_t \lambda / 4)^{1/3}$.

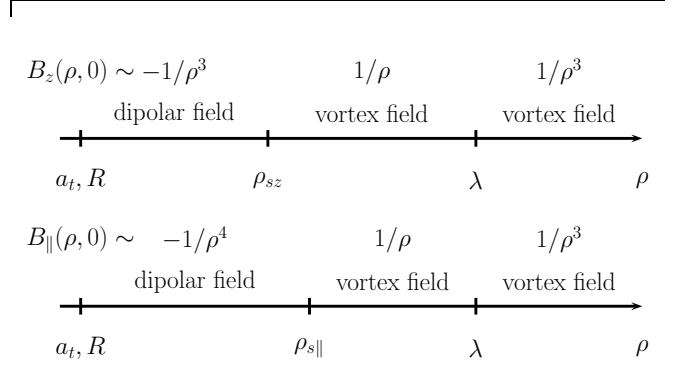


FIG. 3: Behavior of the magnetic field near the upper film surface. Magnetization of the dot is assumed to be directed as in Fig. 1 such that a single vortex appears under the dot. The magnetic field changes the sign at some distance from the dot due to the presence of the vortex.

Qualitatively different behavior of the normal and parallel magnetic field is summarized in Fig. 3 when a single vortex is present in the GS. Sufficiently close to the dot dominates the dipolar field from the dot, while at larger distances the vortex part of the field is a leading term.

So far we have only considered a single vortex under the dot. Since there may be many other vortex–antivortex states in the film, the magnetic field (vortex part only) of such configurations behaves differently than in (16) and (17) and will get angular dependence. We do not analyze this case. Again, the total magnetic field close enough to the dot will be dominated by the dipolar field from the dot, while at larger distances the anisotropic vortex part of the magnetic field prevails. One should be able to use the measurement of magnetic field near the film for detection of many–vortex states bounded by the dot.

V. NUMERICAL STUDY OF GROUND STATES WITH LOW NUMBER OF VORTICES

In section III we have shown analytically a possibility of having a vortex–antivortex pair in the GS. That was the simplest GSC with antivortex. Certainly there are other more complicated states for a range of parameters. Analytic study of these states is in principle straightforward using already introduced expressions, but tedious.

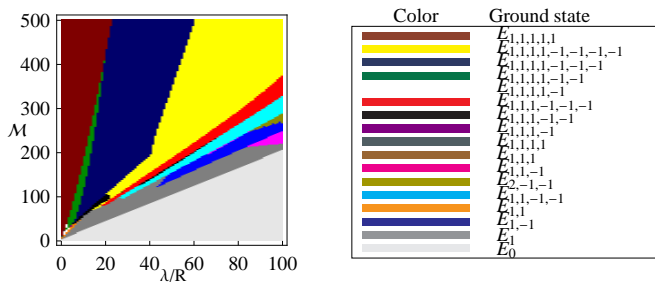


FIG. 4: (Color online) Phase diagram of a magnetic dot for $L = 6$ and $a_t/R = 0.01$ with different vortex–antivortex configurations.

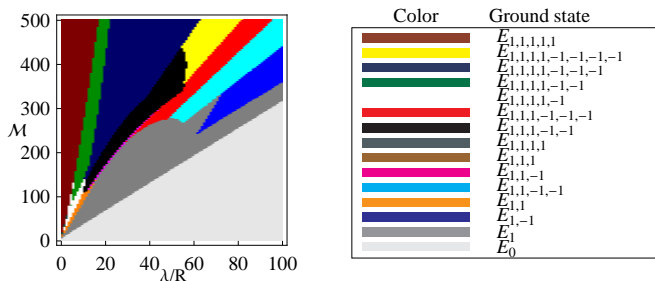


FIG. 5: (Color online) Phase diagram of a magnetic dot for $L = 6$ and $a_t/R = 1$ with different vortex–antivortex configurations.

In this section we study numerically GSCs. For a given configurations uniquely determined by n_1, n_2, \dots we use expression (1) to obtain the energy minimum and positions of vortices and antivortices. The GSC for given λ/R , a_t/R , L and \mathcal{M} has the energy minimum over of all possible vortex–antivortex configurations. In our calculations we took into account just states with low numbers of vortices, since they cover significant part of the parameter space as well as the other states are computationally demanding. Dot–magnet distance is set to $d = 0$. We have examined all states which have up to four vortices with antivortices, while for the states with five vortices we took into account vortices without antivortices. This is certainly not correct since antivortices appears in states with five vortices as well, but such states are located in a particular region of the parameter space and do not affect states with up to three vortices (see further in the text).

States with six and more vortices are not taken into account. This is not crucial for our study since the vortex state with vorticity n will appear in the phase diagram for $\mathcal{M} \geq 2n\lambda/R$ which is either for large magnetization or large magnetic dots (with respect to λ). On the other hand line with n single vortices (and antivortices) is moved a little bit toward smaller \mathcal{M} for a given λ/R .

In Fig. 4 we show the GSC of the magnetic dot with $a_t/R = 0.01$ and $L = 6$. For low \mathcal{M} there are no vortices in the GS for any λ/R . With increasing \mathcal{M} state E_1 appears. Further increase of \mathcal{M} is ultimately followed

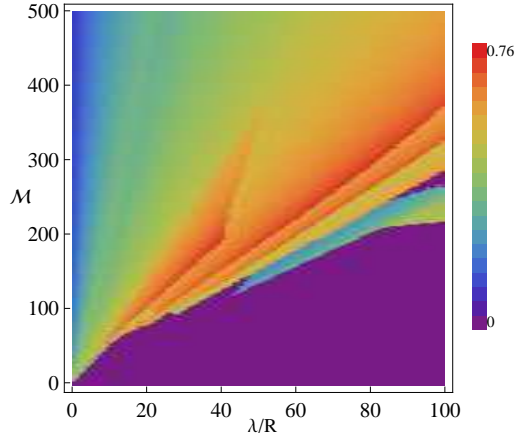


FIG. 6: (Color online) Vortex distances (in units of dot radius R) from the dot center for $L = 6$ and $a_t/R = 0.01$ which correspond to a particular ground state configuration given in FIG. 4.

with the antivortex appearance in the GS. To be concrete let us consider $\lambda/R = 50$. After E_1 , state with antivortex $E_{1,-1}$ appears which is the GSC for some region of \mathcal{M} . Then states $E_{1,1,-1,-1}$, $E_{1,1,1,-1,-1,-1,-1}$, $E_{1,1,1,1,-1,-1,-1,-1}$ appear for larger \mathcal{M} . Further states might have included states with five vortices with antivortices if we had taken them into account. We see that states that evolve from each other have vortex and/or antivortex more/less with respect to its neighbors. We believe that this should mean that states with three vortices will not be affected by the states with five vortices.

Also the net vorticity of the GSCs is in general small ($0, \pm 1$), just near the origin it is higher. However for small λ/R the dot radius is pretty large for realistic films and further analysis with finer resolution of λ/R is necessary. We are here mainly concentrated in the region where $R < \lambda$ since it is the most interesting experimentally, see the last section for some numerical values of parameters.

The distance between the center of the dot and vortices and antivortices are shown in Fig. 6 and Fig. 7 respectively. We see that they abruptly change at boundaries between different GSCs. We also see that antivortices when are present are at distances of a few R . Inside the same GSC for fixed λ/R with increasing \mathcal{M} the antivortices spread, while vortices shrink. This is plausible: very large magnetization of the dot would expel antivortices to very large distances since the interaction energy cannot be then compensated by the attractive vortex–antivortex attraction. On the other hand vortices are attracted at smaller distances toward the potential minimum of the vortex–magnet interaction. These results are also confirmed by analytic formulae (12) and (13) from the study of a single pair.

We also find that in states with zero total vorticity and

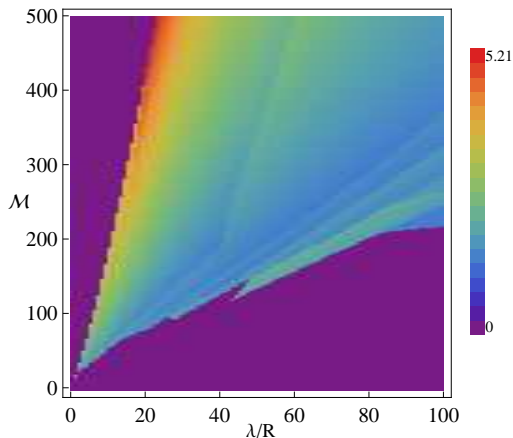


FIG. 7: (Color online) Antivortex distances (in units of dot radius R) from the dot center for $L = 6$ and $a_t/R = 0.01$ which correspond to a particular ground state configuration given in FIG. 4.

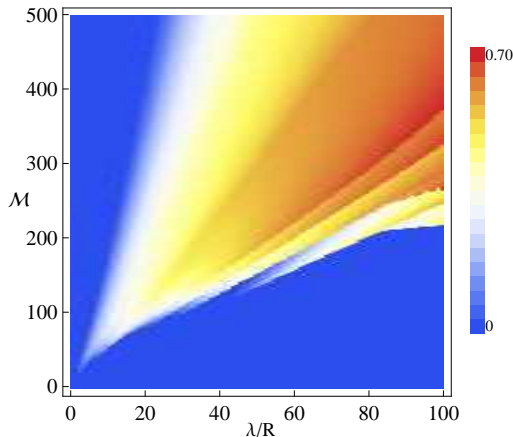


FIG. 8: (Color online) Relative energy change in the ground state when antivortices are included for $L = 6$ and $a_t/R = 0.01$.

two, three and four vortices, positions of antivortices are obtained as homothetically transformed positions of vortices, and they form line, equilateral triangle and square, respectively.

The GSCs without antivortices are shown in Fig. 9. Relative energy difference due to the presence of antivortices is shown in Fig. 8. The relative energy gain is quite significant which means that states without and with antivortices have quite different energies.

We see from Fig. 8 that for smaller magnetization the vortex states with single vortices appear, while state with double vortex E_2 is present for higher \mathcal{M} . Simple analytical check gives that condition $E_{1,1} \leq E_2$ translates

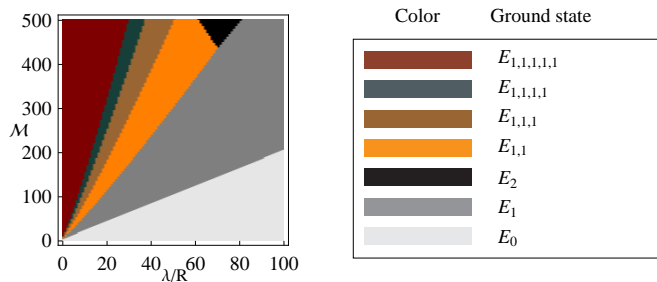


FIG. 9: (Color online) Phase diagram of a magnetic dot for $L = 6$ and $a_t/R = 0.01$ without antivortices.

into

$$\mathcal{M} \leq \frac{1}{L} \exp(2L + 1 - 2\gamma) \frac{R}{\lambda}, \quad (26)$$

which for $L = 6$ becomes $\mathcal{M} \leq 23200R/\lambda$. That also gives one explanation why the only ground state with giant vortices in Fig. 4 is $E_{2,-1,-1}$: it appears around $\lambda/R = 100, \mathcal{M} = 250$ in agreement with rough estimate (26). The other states with giant vortices may appear only for higher $\mathcal{M}\lambda/R$ ratios.

For comparison with thicker magnetic dots we have calculated the GS for $a_t/R = 1$ and they are shown in Fig. 5. The single vortex appears now for larger \mathcal{M} , which is obvious from (7). State $E_{1,-1}$ now occurs for larger λ/R . However a global picture with diversity of vortex-antivortex states again holds. However GSC here are shifted toward higher λ/R and \mathcal{M} values with respect to the corresponding states for thinner dots. We may interpret this as a fact that thicker magnets are less efficient in exciting vortices which is due to the larger extent of the dot with respect to the film surface. Very thick dots ($a_t \gg R$) interact with vortices weakly, see two cases in formula (3).

Now we comment about the applicability of the London approximation for our case. The dot radius over the coherence length ξ as a function λ/R is given as $R/\xi = R \exp(L + \gamma)/(4\lambda)$. We may conclude that for $\lambda/R < 100$ and $L = 6$ the dot radius is always larger than the coherence length. On the other hand a necessary condition for the London approach to be valid is that all lengths are (much) larger than the coherence length. We see that this is satisfied better as λ/R approaches smaller values. We expect that our results with different GSCs are valid even qualitatively for $\lambda/R \lesssim 50$, while the general picture with antivortices and low vorticity GSC holds even for smaller dot radii. However it is expected that for smaller R/ξ ratios, giant vortices are favorable. We have already mentioned such tendency.

Let us mention that a certainly better numerical way would be the nonlinear Ginzburg-Landau theory. For the case of mesoscopic superconducting discs comparison of these two methods shows that both methods give similar results for $R = 6\xi$ and up to five vortices.²⁵

VI. DISCUSSIONS AND CONCLUSIONS

Let us consider numerical values of parameters for realistic systems. For thin Nb films close to the critical temperature $T/T_c = 0.98$ values for the London penetration depth and the coherence length are $\lambda_L \cong 560$ nm and $\xi \cong 58$ nm.²⁶ Then $L = 6$ corresponds to a film of thickness $d_s \cong 30$ nm with the effective penetration depth $\lambda \cong 10.5 \mu\text{m}$. Condition for $E_{1,-1}$ state (11) can be rewritten as $R < \lambda_L \sqrt{\xi/(9d_s)}$ or in our case $R < 260$ nm. The condition for the applicability of the London theory $\xi < R$ is still satisfied, so the results should be valid. Larger magnetic dots may have other vortex–antivortex configurations, and the London theory is expected to be applicable.

In this paper we have considered infinite films. We expect this not to be a severe limitation as soon as the dot radius is much smaller than the system size since the antivortices when appear are at distances of the order of R and the boundaries of the film should not affect it. For films with lateral dimensions smaller than λ the single vortex energy, Eq. (6) will have under the logarithm the lateral dimension instead of 4λ , and for small dot radii essentially the same story should be repeated, just with new U_v .

To conclude, in this paper we have considered a thin superconducting film with a cylindrical magnetic dot with permanent magnetization upon it. Inside the Maxwell–London approach we have calculated the vortex–magnet interaction as well its asymptotic limits. Using these results we have shown analytically that a vortex–antivortex pair appears in the ground state of the system for some range of dot’s radii and its magnetization. Necessary magnetization for that is comparable to the magnetization for the appearance of a single vortex. Magnetic field everywhere in space is also calculated. Near the film surface, the magnetic field has different scaling forms with the distance from the dot center. This fact may be used for the experimental detection of vortices. In addition to that we have calculated numerically the phase diagram with up to four vortices with antivortices.

Acknowledgments

This work is financially supported by the DFG under the grant NA222/5-2 and partly by the DOE under the grant DE-FG02-06ER46278. The author wishes to thank Prof. V. Pokrovsky for many fruitful discussions and Prof. T. Nattermann for his support.

VII. APPENDIX

In this appendix we calculate asymptotically the integrals that appears in the interaction energy (2). We consider an integral of the form

$$I(a, b, c) = \int_0^\infty dx J_0(ax) J_1(x) \frac{\exp(-cx)}{x(1+2bx)}. \quad (27)$$

In the limit $a \gg c$ and $a \gg 1$ this integral will be cut by the oscillations of the Bessel functions and the main contribution comes from the region $x < 1/a \ll 1$. Then we can expand $J_1(x) \exp(-cx) \approx x(1-cx)/2$. Using the tabulated integrals²⁷

$$\int_0^\infty dx \frac{J_0(\alpha x)}{1+x} = \frac{\pi}{2} [H_0(\alpha) - Y_0(\alpha)], \quad (28)$$

$$\int_0^\infty dx J_0(\alpha x) = \frac{1}{\alpha}, \quad (29)$$

we easily get

$$I(a, b, c) = \frac{2b+c\pi}{8b^2} \frac{\pi}{2} \left[H_0\left(\frac{a}{2b}\right) - Y_0\left(\frac{a}{2b}\right) \right] - \frac{c}{4ab}. \quad (30)$$

Using the expansion²¹

$$\frac{\pi}{2} [Y_0(x) - H_0(x)] = \begin{cases} \gamma + \log \frac{x}{2} - x, & x \ll 1 \\ -x^{-1} + x^{-3}, & x \gg 1 \end{cases} \quad (31)$$

where $\gamma \approx 0.577$ is the Euler constant, one can further simplify the asymptotic expressions for $I(a, b, c)$.

In the limit $a \ll c$ and $a \ll 1$ integral (27) is cut by the exponential function at $x \approx 1/c$, which means the argument of J_0 function $ax \approx a/c \ll 1$ and we expand $J(0, ax) \approx 1 - a^2 x^2/4$. We get

$$I(a, b, c) = \int_0^\infty dx J_1(x) \exp(-cx) \times \left(-\frac{a^2}{8b} + \frac{1}{x} + \frac{\frac{a^2}{8b} - 2b}{1+2bx} \right). \quad (32)$$

Then using the tabulated integrals²⁷

$$\int_0^\infty dx \frac{J_1(\alpha x)}{1+x} = 1 + \frac{1}{\alpha} + \frac{\pi}{2} [Y_1(\alpha) - H_1(\alpha)], \quad (33)$$

$$\int_0^\infty dx J_1(\alpha x) \frac{\exp(-\gamma x)}{x} = -\gamma + \sqrt{1+\gamma^2}, \quad (34)$$

$$\int_0^\infty dx J_1(\alpha x) \exp(-\gamma x) = 1 - \frac{\gamma}{\sqrt{1+\gamma^2}}, \quad (35)$$

and the expansion for $x \ll 1$ ²¹

$$\frac{\pi}{2} [H_1(x) - Y_1(x)] = \frac{1}{x} + \frac{x}{4} \left(1 - 2\gamma + \log \frac{4}{x^2} \right) \quad (36)$$

we get for $a \ll c \ll 1 \ll b$

$$I(a, b, c) = \frac{1}{8b} \left(1 - 2\gamma + c(a^2 - 4) - a^2 \sqrt{1+c^2} + \log \frac{16}{b^2} \right) + c - \frac{c}{\sqrt{1+c^2}}. \quad (37)$$

In the above expressions J_0 and J_1 are the Bessel functions of the first kind, Y_0 and Y_1 are the Bessel functions of the second kind, while H_0 and H_1 are the Struve functions of order zero and one, respectively.²¹

-
- ¹ M. Tinkham, *Introduction to superconductivity* (McGraw-Hill, 1996).
- ² G. Blatter, M. V. Feigel'man, V. B. Geshkenbein, A. I. Larkin, and V. M. Vinokur, *Rev. Mod. Phys.* **66**, 1125 (1994).
- ³ A. A. Abrikosov, *Sov. Phys. JETP* **5**, 1174 (1957).
- ⁴ J. Pearl, *Appl. Phys. Lett.* **5**, 65 (1964).
- ⁵ A. L. Fetter and P. C. Hohenberg, *Phys. Rev.* **159**, 330 (1967).
- ⁶ D. S. Fisher, *Phys. Rev. B* **22**, 1190 (1980).
- ⁷ I. F. Lyuksyutov and V. L. Pokrovsky, *Adv. in Phys.* **54**, 67 (2005).
- ⁸ M. Vélez, J. I. Martín, J. E. Villegas, A. Hoffmann, E. M. González, J. L. Vicent, and I. K. Schuller, *J. Magn. Magn. Mater.* **320**, 2547 (2008).
- ⁹ J. I. Martín, M. Vélez, J. Nogués, and I. K. Schuller, *Phys. Rev. Lett.* **79**, 1929 (1997).
- ¹⁰ D. J. Morgan and J. B. Ketterson, *Phys. Rev. Lett.* **80**, 3614 (1998).
- ¹¹ I. F. Lyuksyutov and V. L. Pokrovsky, *Phys. Rev. Lett.* **81**, 2344 (1998).
- ¹² R. Sasik and T. Hwa, arXiv:cond-mat/0003462 (2000).
- ¹³ S. Erdin, A. M. Kayali, I. F. Lyuksyutov, and V. L. Pokrovsky, *Phys. Rev. B* **66**, 014414 (2002).
- ¹⁴ S. Erdin, *Phys. Rev. B* **72**, 014522 (2005).
- ¹⁵ M. V. Milošević and F. M. Peeters, *Phys. Rev. B* **68**, 024509 (2003).
- ¹⁶ I. K. Marmorkos, A. Matulis, and F. M. Peeters, *Phys. Rev. B* **53**, 2677 (1996).
- ¹⁷ M. V. Milošević, S. V. Yampolskii, and F. M. Peeters, *Phys. Rev. B* **66**, 174519 (2002).
- ¹⁸ S. Erdin, in *Frontiers in Superconducting Materials*, edited by A. Narlikar (2005), p. 425.
- ¹⁹ L. F. Chibotaru, A. Ceulemans, V. Bruyndoncx, and V. V. Moshchalkov, *Nature (London)* **408**, 833 (2000).
- ²⁰ L. F. Chibotaru, A. Ceulemans, V. Bruyndoncx, and V. V. Moshchalkov, *Phys. Rev. Lett.* **86**, 1323 (2001).
- ²¹ M. Abramowitz and I. A. Stegun, *Handbook of Mathematical Functions* (Dover, New York, 1972).
- ²² J. Pearl, in *Low Temperature Physics-LT9*, edited by J. G. Daunt, D. O. Edwards, F. J. Milford, and M. Yagub (1965), p. 566.
- ²³ A. A. Abrikosov, *Introduction to the theory of metals* (North-Holland, 1988).
- ²⁴ J. D. Jackson, *Classical Electrodynamics* (John Wiley and Sons, New York, 1975), 2nd ed.
- ²⁵ B. J. Baelus, L. R. E. Cabral, and F. M. Peeters, *Phys. Rev. B* **69**, 064506 (2004).
- ²⁶ A. Hoffmann, P. Prieto, and I. K. Schuller, *Phys. Rev. B* **61**, 6958 (2000).
- ²⁷ A. P. Prudnikov, Y. A. Brychkov, and O. I. Marichev, *Integrals and Series* (Gordon and Breach Science Publishers, Amsterdam, 1986).